PERGAMON

Journal of Structural Geology 22 (2000) 1165–1179

JOURNAL OF STRUCTURAL GEOLOGY

www.elsevier.nl/locate/jstrugeo

Modelling hanging wall accommodation above rigid thrust ramps

Marco Bonini[a,*], Dimitrios Sokoutis[b], Genene Mulugeta[c], Emmanouil Katrivanos[b]

[a]*CNR-Centro di Studio di Geologia dell'Appennino e delle Catene Perimediterranee, Analogue Modelling Laboratory, via G. La Pira 4, I-50121 Firenze, Italy*

[b]*Aristotle University of Thessaloniki, School of Geology, Department of Geology and Physical Geography, GR-54006 Thessaloniki, Greece*

[c]*Hans Ramberg Tectonic Laboratory, Institute of Earth Sciences, Uppsala University, Norbyvägen 18B, S-75236 Uppsala, Sweden*

Received 29 July 1999; accepted 30 March 2000

Abstract

Experimental models are used to study the role of material rheology in hanging wall accommodation above rigid flat–ramp–flat thrust footwalls. The deformation in the hanging wall was accomplished by forwards sliding along a rigid basal staircase trajectory with a variable ramp angle, α, ranging from 15° to 60°. We model different ramp angles to examine hanging wall accommodation styles above thrust ramps of overthrust faults (α ranging from 15° to 30°), as well as above pre-existing normal faults (α ranging from 45° to 60°). For the hanging walls we used stratified frictional (sand) and viscous (silicone putty) materials.

In this paper we study three types of models. Type 1 models represent purely frictional hanging walls where accommodation above thrust ramps was by layer-parallel thickening and by generating a series of back thrusts.

Type 2 and 3 models represent stratified frictional/viscous hanging walls. In these models, accommodation was by a complex association of reverse and normal faults, mainly controlled by the rheological anisotropy as well as by the ramp inclination angle α. In Type 2 models the silicone covered only the lower flat, while in Type 3 models it also covered the rigid ramp. For $\alpha \leq 30°$ in Type 2 models and $\alpha \leq 45°$ in Type 3 models, the viscous layer inhibited the development of back thrusts in the frictional hanging wall, instead the silicone thickened to develop a 'ductile ramp'. For α-values higher than 30° in Type 2 models and $\alpha = 45°$ in Type 3 models, back thrusts develop in response to the bulk compression.

The experiments simulate many structures observed above natural thrust ramps with $\alpha \leq 30°$ and pre-existing normal faults with $\alpha \geq 45°$. The models emphasise the importance of a basal ductile layer, which allows the hanging wall to step-up over the rigid ramp by building up its own ductile ramp. The models also emphasise that foreland-directed normal faulting can develop at a thrust front in the case that the vertical stress due to gravity exceeds the horizontal stress due to end-loading within a thrust wedge.

1. Introduction

Thrust sheets are generally composed of incompetent and competent horizons forming a brittle–ductile multilayer system. Upon shortening, this system develops thrust faults characterised by ramp–flat geometry, with the flats commonly localised along the incompetent horizons and the ramps cutting upsection through the competent layers (Dahlstrom, 1970; Elliott, 1976; Harris and Milici, 1977; Berger and Johnson, 1980; Boyer and Elliot, 1982; Butler, 1982; Carter and Hansen, 1983; Mitra, 1986; Eisenstadt and De Paor, 1987, among others). Ductile layers, such as salt and shale, are widespread in natural thrust systems, such that they commonly constitute the preferred basal detachment layer for emplacement of the thrust sheets (e.g. Gretener, 1972, 1981; Davis and Engelder, 1985; Cello and Nur, 1988). Accommodation styles in natural hanging walls, which develop above frontal thrust ramps, have been described in detail from several natural examples (e.g. Rich, 1934; Serra, 1977; Wiltschko, 1979, 1981; Suppe, 1983; Bombolakis, 1986; Cooper

* Corresponding author. Fax: +39 055 2302302.
E-mail address: mbonini@geo.unifi.it (M. Bonini).

0191-8141/00/$ - see front matter
PII: S0191-8141(00)00033-X

and Trayner, 1986; Beutner et al., 1988; Taboada et al., 1990; Jordan and Noack, 1992, among others).

Many fold-and-thrust-belts share the occurrence of normal faults in layered sedimentary sequences prior to thrusting. The evolution of rifted continental margins is typically accompanied by the development of normal faults displacing the sedimentary sequences. These faults can juxtapose layers with different mechanical behaviour (e.g. evaporites vs. limestones or sandstones), giving rise to strong lateral rheological variations (e.g. Butler, 1989; Tavarnelli, 1996). Additionally, syn-depositional activity of normal faults can control the accumulation of thick evaporite sequences on the hanging wall, which can play an important role during later shortening events.

The mechanics of frontal ramp accommodation has also been investigated by analogue modelling (e.g. Merle and Abidi, 1995). These models demonstrated the control on ramp accommodation of both friction along the ramp and erosion of the growing hanging wall relief.

In the present paper we investigate experimentally the mechanics of internal deformation of thrust sheets which develop above thrust ramps with a variable ramp angle, named α. Firstly, we explore hanging wall accommodation styles in purely brittle systems. We then investigate accommodation in rheologically stratified brittle–ductile systems, where a frictional material overlies a basal viscous layer. We vary the frontal ramp angle, α, and use it as a rigid indentor to deform the frictional or stratified viscous/frictional hanging walls (Fig. 1a). We take into consideration different aspects of the models such as initiation, maturity and late stages of deformation of the thrust sheets in order to compare the experimental results with natural examples. We emphasise the changes in the internal geometry of the thrust sheets during deformation depending on the initial geometrical configuration such as ramp inclination angle and ratio of viscous to frictional layering.

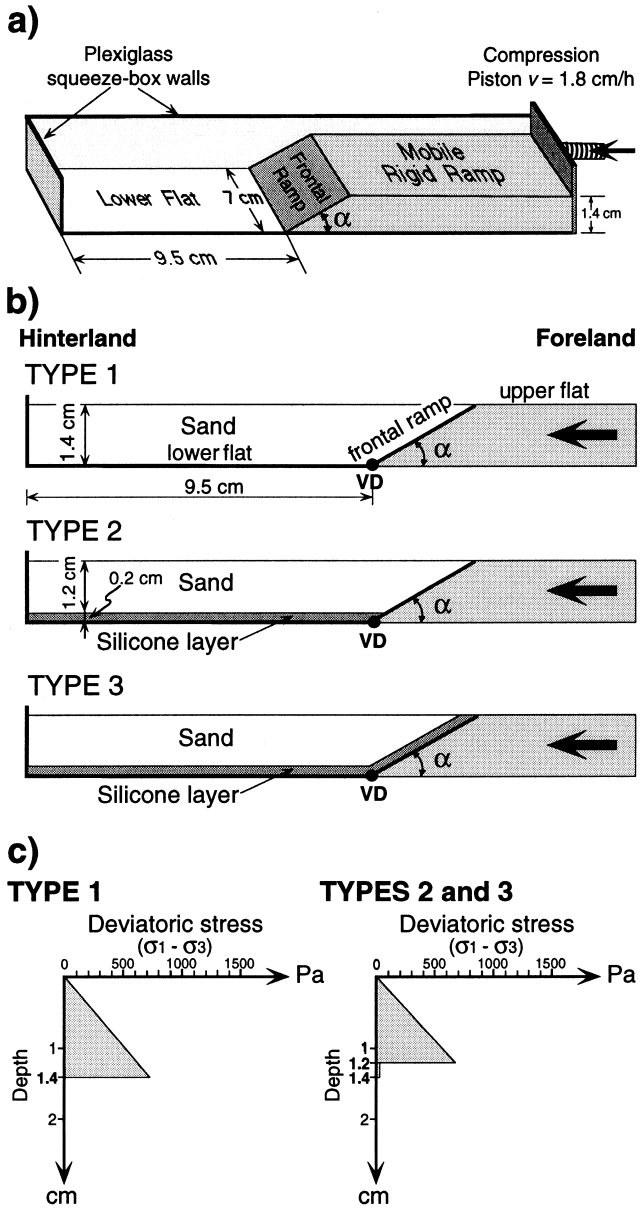

Fig. 1. (a) Model set-up and (b) definition of nomenclature used in the text; VD: velocity discontinuity. (c) Deviatoric stress of brittle material (sand) has been calculated following Weijermars (1997) (his equation 6-5a for compressional regime). The strength profile of viscous material (silicone) is based on the mean strain-rate of the experiment (1.25×10^{-4} s^{-1}).

2. Method and experimental procedure

2.1. Model construction and deformation

Our experiments were performed at the Hans Ramberg Tectonic Laboratory of the Institute of Earth Sciences of Uppsala, at the Analogue Modelling Laboratory of the CNR-CSGACP at the Department of Earth Sciences in Firenze and at the Tectonic Laboratory of the Aristotle University of Thessaloniki.

Three types of models have been investigated (Fig. 1b): Type 1 models with purely frictional hanging walls, Type 2 models with stratified sand–silicone layering, where a basal silicone layer rests only above the lower flat, and Type 3 models with stratified sand–silicone layers where a basal silicone layer covers both the lower flat and the frontal ramp sector.

Models were built in a Plexiglas squeeze box with dimensions 9.5 cm × 7 cm ×1.4 cm. Coloured sand layers were sedimented as passive markers to visualise the internal deformation. The thickness of the sand layers varied according to the different geometries of the models. The maximum thickness of the sand was 1.4 cm in the purely brittle systems (Type 1); the thick-

ness of the basal silicone layer remained constant, 0.2 cm, irrespective of the type of experiment, so that the brittle/ductile thickness ratio was 6 (see Fig. 1a and b). Both the base and the sides of the silicone were lubricated with liquid soap so as to minimise boundary friction.

Models were shortened by pushing a rigid ramp block with a frontal dip (angle α) varying from 15° to 60°, at increments of 15°. The rigid ramp was driven by an electric motor, at a constant rate of convergence of 1.8 cm h^{-1}. Models were commonly shortened up to 40% bulk shortening (%BS), though in some cases a wider range of bulk shortening was explored (i.e. varying from 20% up to 80% for Type 1 models and $\alpha = 30°$). However, these models do not explore the role of erosion and syntectonic redistribution of the sand.

Photographs of the models were taken at constant time intervals during deformation. After deformation, models were covered by dry sand to preserve the final topography, then models were soaked in water and frozen before taking cross-sections, i.e. without disturbing the model.

2.2. Model materials

Two analogue materials have been used in this experimental investigation (Fig. 1): the frictional material consisted of pure quartz sand with particle diameters less than 0.246 mm and the viscous material was represented by silicone bouncing putty, Rhodosil Gomme GSIR (RG 70009), supplied by Rhône Poulenc of Paris.

The sand is a Mohr–Coulomb material with a mean density $\rho_b = 1300$ kg/m^3, which simulates the brittle behaviour of sedimentary rocks. In laboratory tests this material shows an angle of internal friction $\phi = 30°$, a coefficient of internal friction $\mu = 0.58$ and a cohesion $c = 105$ Pa. The silicone putty exhibits Newtonian behaviour and represents ductile rocks in nature (e.g. evaporites, shales) which may be located either at the base of the thrust sheet and/or interbedded within competent rocks composing the thrust sheet.

The density of the silicone putty utilised in this investigation was $\rho_d = 1160$ kg/m^3 and the viscosity $\eta = 4 \times 10^4$ Pa s (at room temperature, ~20°C). The silicone was deformed at a mean bulk strain-rate of $\varepsilon_m = 1.25 \times 10^{-4}$ s^{-1}, which has been calculated as the ratio between the velocity of the moving rigid ramp (1.8 cm h^{-1}) and the average length (about 4 cm) of the thickened silicone wedge that developed in front of the rigid ramp (see later).

2.3. Scaling of the models

Scaling of the sand models to natural conditions is necessary for evaluating the experimental results (Hubbert, 1937). The scaling was performed by using the model ratio of stress. In purely brittle hanging walls (Type 1), the model to nature scale (length) ratio $h^* = h_m/h_n$ can be obtained from the Coulomb criterion, which predicts the rheological behaviour of rocks at upper crustal levels:

$$\tau = \mu\sigma + c \quad (1)$$

where τ and σ are the shear and normal stresses on the fault plane, respectively, $\mu = \tan\phi$ the coefficient of friction, ϕ the angle of internal friction and c the cohesion of the brittle material. Dividing Eq. (1) by σ and substituting $\sigma = \rho g h$, gives:

$$\frac{\tau}{\rho g h} = \mu + \frac{c}{\rho g h}$$

where ρ is density, g is the acceleration due to gravity and h is the height of the thrust sheet. A similar τ/σ ratio between model (m) and nature (n) implies that:

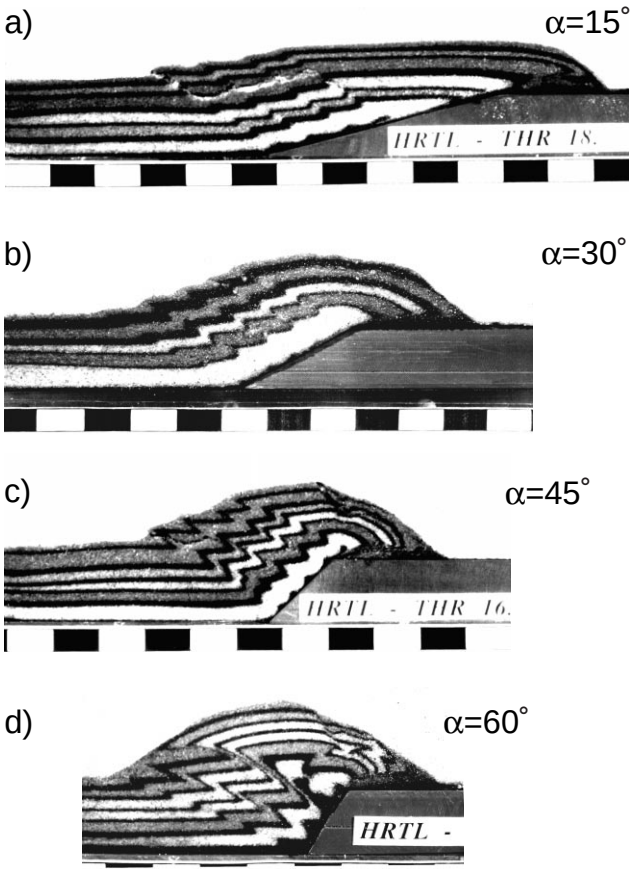

Fig. 2. Cross-sections of experiments with frictional hanging wall (Type 1) at 40% bulk shortening. Frontal ramp angle ranges from 15° up to 60° by steps of 15°. The ruler at the base of all models is in centimetres.

$$\mu_m + \frac{c_m}{\rho_m g h_m} = \mu_n + \frac{c_n}{\rho_n g h_n}$$

μ_m and μ_n have a similar value ($\mu_m \approx 0.6$ and μ_n ranges between 0.6 and 0.85, e.g. Byerlee, 1978; Weijermars et al., 1993) and can be neglected in the above equation, so we obtain:

$$h^* = \frac{h_m}{h_n} = \frac{\rho_n c_m}{c_n \rho_m} \quad (2)$$

substituting the parameters of Table 1 in Eq. (2), we obtain $h^* = h_m/h_n = 4.8 \times 10^{-6}$, which implies that the model (1.4 cm thick) represents a natural thrust sheet with a basal detachment about 3 km deep. Similarly, the ratio between normal stress in the model (m) and in nature (n) σ_m/σ_n is $\sigma^* = \rho^* g^* h^* = 2.6 \times 10^{-6}$, while the horizontal displacement rate v^* is given by the product of ε^* and l^* (e.g. Merle and Abidi, 1995), so that $v^* = v_m/v_n = 6 \times 10^4$. From this we can say that the velocity of the piston, $v_m = 1.8$ cm h^{-1}, corresponds to a velocity $v_n = 2.6$ mm y^{-1}, which is comparable to that observed in natural thrust systems (e.g. Kukal, 1990; Allen et al., 1991; Merle and Abidi, 1995; Zapata and Allmendinger, 1996).

3. Experimental results

3.1. Type 1: Purely frictional hanging wall

In purely frictional hanging walls, shortening of the sand models was accommodated by formation of a series of back thrusts (Fig. 2). The first structures to appear were back thrusts, which nucleated at the base of the ramp. We refer to these structures as 'back thrusts' because they move in opposite sense with respect to the forward sliding of the hanging wall along the basal staircase trajectory. As the deformation continued, the earlier back thrusts migrated along the ramp while new ones developed serially at the base of the ramp. A similar geometry also results in the experiments on thrust sheet emplacement performed by Colletta et al. (1991) and Merle and Abidi (1995).

In the experiments illustrated here, four back thrusts typically formed (after 40% bulk shortening) for α values ranging from 15 to 45° during frictional gliding. Spacing between the serially nucleating back thrusts was regular for a given α angle, decreasing with increasing α, whereas slip along the faults increased as α increased (Fig. 2). At $\alpha = 60°$ a pair of back- and fore thrusts developed in the sand wedge emanating from a point slightly shifted in front of the toe of the rigid ramp. This process gave rise to a 'pop-up' structure, causing an upward escape of material in response to movement along the two step-up shear zones (Fig. 2d). Both the fore- and back thrusts show a convex upward geometry. These become accentuated with time so as to allow the system to accommodate the lateral spreading of the sand wedge.

In all these experiments, the active back thrusts nucleated (at the base of the ramp) as kink bands, whose width decreased with increased shearing. This process can be related to shear softening and localisation along the shear zone as discussed by Mulugeta and Koyi (1992). This effect was greatest for $\alpha = 60°$, since fewer (three) back thrusts formed to accommodate the deformation (Fig. 2d).

To investigate the effect of a wider range of bulk shortening, four experiments with bulk shortening (BS) varying from 20% to 80% at steps of 20% were performed for $\alpha = 30°$ (Fig. 3). Typically the first back thrust appeared at the surface after 3.1% BS. At a low value of bulk shortening, the model profile exhibited a

Table 1
Analogue modelling parameters[a]

Parameter	Model	Nature	Model/Nature ratio
BL Density, ρ_b (kg m^{-3})	1300	2400	0.54
DL Density, ρ_d (kg m^{-3})	1160	2200	0.53
DL Viscosity, η (Pa s)	4×10^4	10^{16}	4×10^{-12}
BL Internal friction coefficient, μ	≈ 0.6	0.6–0.85	
BL Cohesion, c (Pa)	105	40×10^6	2.6×10^{-6}
Strain-rate, ε (s^{-1})	1.25×10^{-4}	10^{-14}	1.25×10^{10}
Gravity acceleration, g (m s^{-2})	9.81	9.81	1
Length, l (m)	0.01	~ 2100	4.8×10^{-6}
Stress, σ (Pa)			2.6×10^{-6}
Time, t (s)	3600	4.5×10^{13} (1.4 Ma)	8×10^{-11}
Rate of displacement, v (m s^{-1})	5×10^{-6}	8.3×10^{-11} (2.6 mm y^{-1})	6×10^4

[a] Model and natural parameters used in the analogue modelling experiments. In the scaling procedure, we have assumed for the natural prototype a mean cohesion $c_n = 40$ MPa (e.g. Hoshino et al., 1972; Weijermars et al., 1993), a typical strain-rate of $\varepsilon_n = 10^{-14}$ s^{-1} and a viscosity $\eta_n = 10^{16}$ Pa s for the natural rock analog (evaporites) at depths similar to that of the scaled models (e.g. Weijermars et al., 1993). BL: brittle layer (sand); DL: ductile layer (silicone).

flat-topped ramp anticline (Fig. 3a), which became progressively more rounded with a convex-upwards geometry (Fig. 3b–d). Foreland-dipping normal faults started to appear at 40% BS, and with increasing bulk shortening, foreland-directed extensional collapse of the sand wedge above the upper flat became increasingly more developed. This process has been markedly accommodated by normal faults partly reactivating older back thrust segments (Fig. 3d) when the latter were transported above the upper flat. The initial back thrusts became reactivated with increasing interlimb angle, ω, of the kink bands (Fig. 3e). The kink interlimb angles increase when the back thrust is re-utilised as a normal fault (cf. Mulugeta and Koyi, 1992). In addition, with increasing shortening the lower sand layer thickened and compacted above the ramp (Fig. 3d) and the back thrust planes became progressively bent during the gliding above the ramp before they became reactivated as normal faults (Fig. 3).

Mechanisms of fault reactivation have been discussed in several papers (e.g. Sibson, 1974, 1985; Jaeger and Cook, 1979; Ranalli and Yin, 1990, among others). Krantz (1991a) and Faccenna et al. (1995) investigated by means of analogue modelling in detail the relations between normal faulting and pre-existing thrust-faults. The angle θ between the σ_1 axis and the

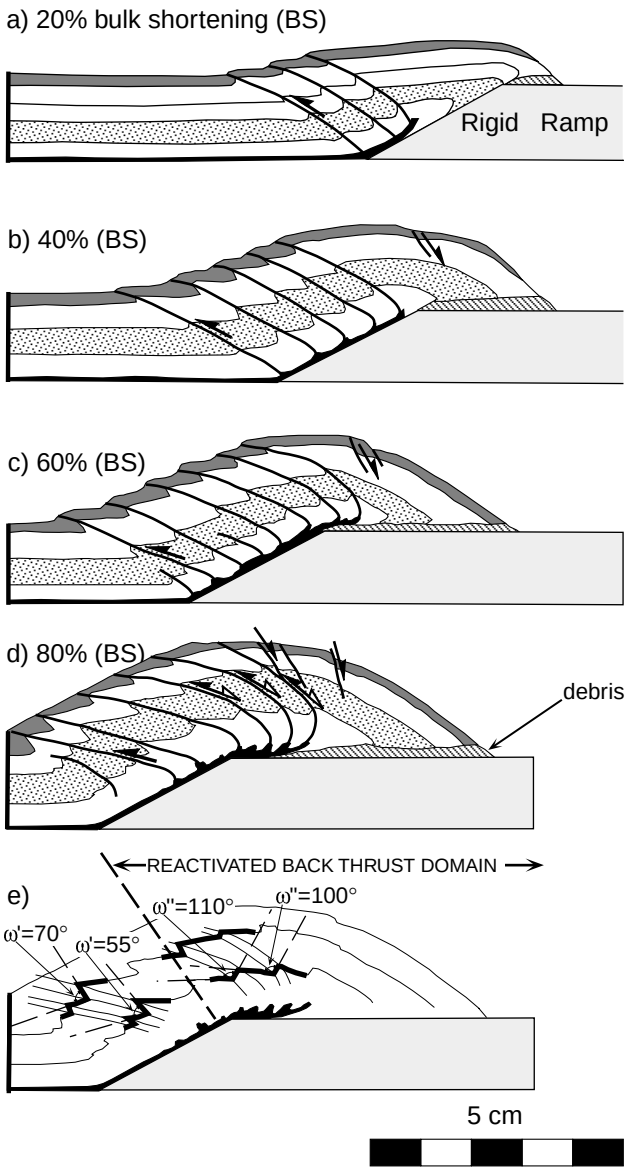

Fig. 3. Type 1 models with $\alpha = 30^\circ$ and bulk shortening ranging from 20% to 80%. The 80% bulk shortening results in the development of a rootless anticline displaying stacked back thrusts above the ramp, which are progressively warped and reactivated as normal faults above the upper flat. These kinematics are reflected by the interlimb angles of kink bands (ω), which are ~55–70° for pure back thrusts (ω') and 100–110° in the reactivated back thrusts (ω''). See text for details.

fault plane is expressed by Anderson (1951):

$$\theta = 45^\circ - \frac{1}{2}\tan^{-1}\mu \quad (3)$$

For $\mu = 0.58$ as in our materials, $\theta \approx 30^\circ$. Therefore, the dip of newly formed normal faults above the upper flat suggests near vertical orientation of the greatest principal stress axis σ_1 (Fig. 4a). The normal faults reactivated the lower part of pre-existing back thrusts, which steepened and rotated to a favourable orientation for normal reactivation.

The range of favourable orientations of pre-existing anisotropies (with respect to the vertical σ_1 axis) within which normal displacement occurred is defined by the minimum and maximum limiting angles, $\alpha = 2.5^\circ$ and $\beta = 59^\circ$, whose values are obtained from graphical solution using the Mohr circle (Fig. 4d; a similar result can be obtained using an analytical solution based on Ranalli and Yin, 1990). This reactivation field is in

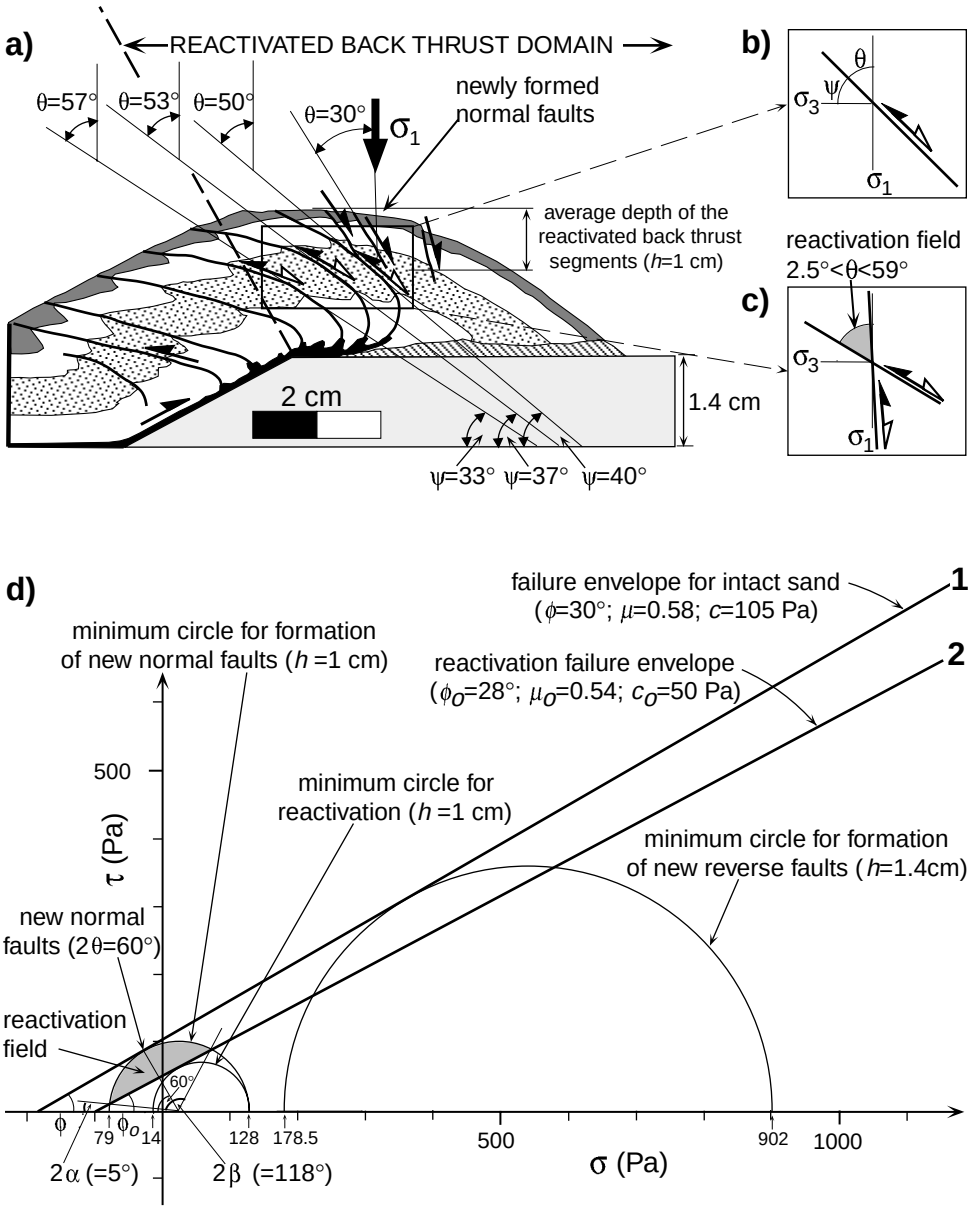

Fig. 4. (a) Extensional reactivation of pre-existing back thrust segments in Type 1, $\alpha = 30^\circ$, and 80% bulk shortening (which is the same figure as that shown in Fig. 3d). Notice that extensional reactivation of the back thrusts occurs contemporaneously with the forward sliding of the hanging wall along the staircase footwall. (b) The inclination θ of the reactivated back thrusts varies between 50° and 57°, falling within the reactivation field (c) predicted by the graphical solution illustrated in (d). (d) Coulomb failure envelope for intact sand ($\rho = 1300$ kg/m^3) used in the models (line 1) and estimated reactivation failure envelope (line 2) assuming for the reactivated sand (sprinkled) a drop in cohesion along the kink bands of about 50% and a drop in the friction coefficient of about 7% (e.g. Krantz, 1991b). Line 1 is from laboratory measurements drawn as best fit by linear regression of τ and σ values at failure.

good agreement with the dip θ of the reactivated back thrust segments which range between 50° and 57° (Fig. 4), thus indicating that the favourably oriented pre-existing back thrusts became reactivated as normal faults as they progressively steepened and entered the reactivation field for normal faulting.

3.2. Type 2: Models with ductile detachment along the lower flat

Cross-sections shown in Fig. 5 illustrate the effects of a basal ductile layer (décollement) on the emplacement of a frictional thrust sheet. In all models with a ductile base the rigid ramp was abandoned as a surface of sliding, and instead the silicone thickened to provide a *ductile ramp* for easy gliding. For $\alpha = 15°$ and 30° no back thrusts developed and the thrust sheets glided simply over the ductile ramp. At $\alpha = 45°$ a number of back thrusts developed during the early stages of shortening, but back thrust development was arrested when the ductile ramp was configured (Fig. 5c). The same analysis also applies to $\alpha = 60°$, with the only difference that a single large back thrust formed; in addition, at $\alpha = 60°$ the ramp anticline assumed a box-fold geometry because of the squeezing of silicone into the core (Fig. 5d).

In all models with a ductile layer along the lower flat the geometry of ramp anticlines also exhibits strong dependence upon the frontal ramp angle. The shape of ramp anticlines seen in profile varies from flat-topped to open as α increases from 15 to 60° (Fig. 5). Growth and collapse of the ramp anticlines on the upper flat gives rise to extensional structures that developed along the crest of the anticlines. The amplitude of ramp anticlines increased with increasing α, resulting in well-developed extensional structures (Fig. 5). At $\alpha = 30°$ a foreland-dipping high-angle normal fault developed (Fig. 5b), whilst at $\alpha = 45°$ (Fig. 5c) the extensional features resulted in the simultaneous

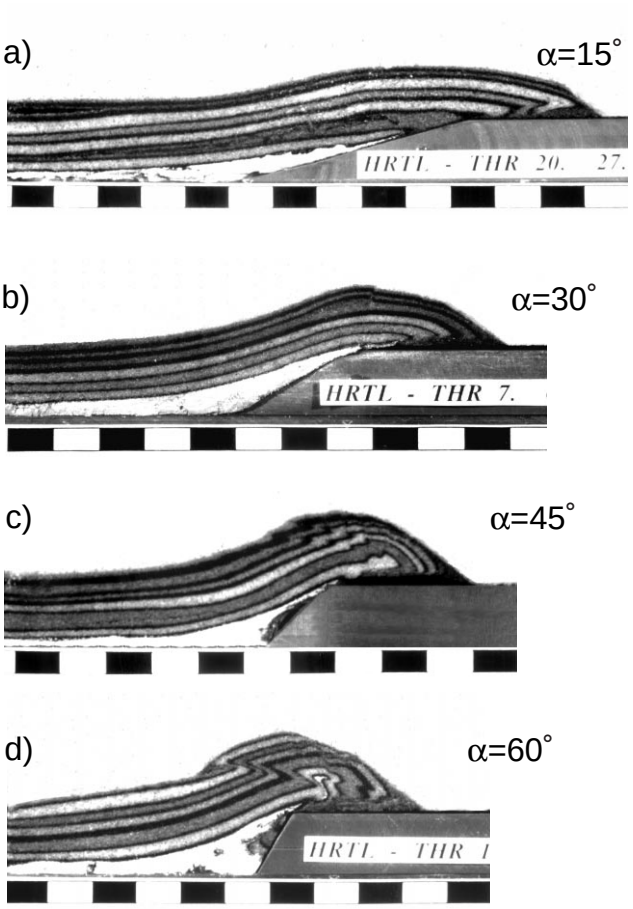

Fig. 5. Cross-sections of experiments with basal detachment layer along the lower flat (Type 2) at 40% bulk shortening. Frontal ramp angle ranges from 15° up to 60° by steps of 15°. The ruler at the base of all models is in centimetres.

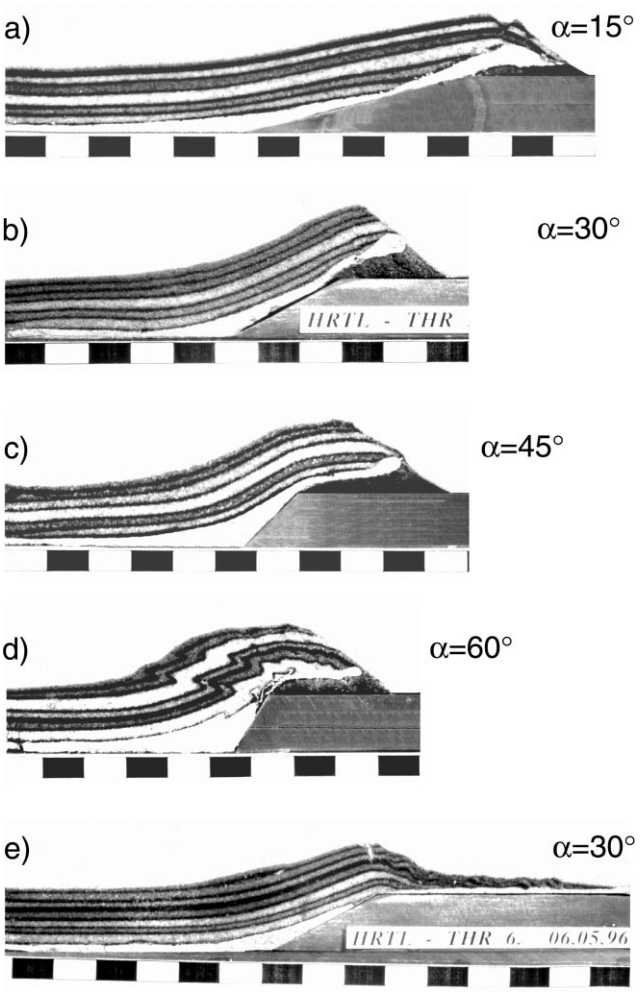

Fig. 6. Cross-sections of experiments with basal detachment layer along both the lower flat and frontal ramp (Type 3) at 40% bulk shortening. Frontal ramp angle ranges from 15° up to 60° by steps of 15°. In (e) is illustrated a particular case where the silicone was initially also laid above the upper flat. The ruler at the base of all models is in centimetres.

development of new normal faults and the reactivation of back thrusts. The latter, as in the Type 1 models shown in Fig. 3, migrated forwards along the ramp, rotated and then were re-utilised as low-angle foreland-dipping normal faults at the upper flat. At $\alpha = 60^\circ$ slip on low-angle normal faults was greater in response to collapse of the ramp anticline at the front, and because no back thrust was available for reactivation (Fig. 5d).

3.3. Type 3: Models with ductile detachment throughout the lower flat and ramp

We investigated the Type 3 models because we wanted to study the control of friction along the ramp for the development of structures in the hanging wall, i.e. the back thrusts. Type 3 experimental model thrust-sheets show similar internal deformation to the Type 2 models, although some differences exist. Both back thrusts and normal faults in Type 3 models were comparatively less developed than in Type 2 models (Fig. 6). Back thrusts developed only at $\alpha = 60^\circ$ and as in the Type 2 models with $\alpha = 45^\circ$, they were then reactivated as low-angle normal faults (Fig. 6d). Apart from a small graben that formed along the crest of the anticline at $\alpha = 15^\circ$ (Fig. 6a), no significant structures (either thrust or normal faults) developed for α ranging from 15° to 45°. Drag of the silicone along the frontal ramp inhibited frictional gliding along the base of the thrust sheets even during the first stages of shortening. However, at $\alpha = 60^\circ$ back-kinks affected the brittle part of the model (Fig. 6d).

A control experiment was also performed but only for $\alpha = 30^\circ$. This involved adding 0.5 cm of silicone above the upper flat with a lubricated base (Fig. 6e). As in the other models with ductile a layer at the base, the frictional hanging wall was not affected by back-kinks and the model evolved a well-developed ramp anticline. The frontal part of the anticline was affected by dramatic normal faulting related to the gravitational collapse and sliding of the overriding thrust sheet along the basal décollement horizon (Fig. 6e).

The geometry of ramp anticlines in Type 3 models was mainly controlled by both the ramp angle α and the initial model configuration. In these models with $\alpha = 30^\circ$ and 45°, the forelimbs of ramp anticlines were normally displaced because of gravitational collapse (Fig. 6b, c). Additionally, at $\alpha = 15^\circ$ and 60° the ramp anticlines displayed a generally smoother geometry as compared to corresponding Type 2 models.

4. Discussion

The series of models illustrate that hanging wall accommodation took place by generating a series of back thrusts in purely frictional hanging walls (Type 1) and by thickening of silicone to produce a ductile ramp in models with viscous basal layers (Types 2 and 3). Localisation of both back-kinks and thickening of the viscous silicone occurred at the toe of the rigid ramp, which therefore represents the main geometrical feature controlling the model deformation. In Type 1 models bulk shortening was accommodated more by layer-parallel shortening at lower levels, and by shear kinking at shallow levels. This process is markedly similar to the accretion geometry in model sand wedges, where the lower sand layers shorten predominantly by layer thickening and lateral compaction while the upper layers accommodate the deformation by kinking and imbrication (e.g. Mulugeta and Koyi, 1992).

In Type 2 and 3 models, migration and thickening of silicone above the toe of the rigid ramp provided a 'ductile (or effective) ramp' upon which the frictional hanging wall could step-up and overthrust the rigid ramp (Fig. 7). In other words, the system spontaneously configured the most efficient geometry for the hanging wall to be thrust over the rigid ramp. No significant thickening was observed in the sand layers overlying the silicone horizon (Figs. 5 and 6), indicating that the frictional hanging wall was transported passively upon the ductile ramp.

Generally, in both Types 2 and 3 models, thickening of the silicone increased with α in order to overcome the steeper ramp dip. This is illustrated by the diagram in Fig. 7(b) where the frontal angle β (arctan dz/dr) of the effective ramp progressively increased with α. Obviously, dz/dr values are higher in Type 3 than in Type 2 models because the silicone layer was also resting on the rigid ramp in the Type 3 initial configuration. In Type 2 models at $\alpha = 60^\circ$, the system isolated a sand pack slice from the footwall to produce the effective ramp (Fig. 5d), whereas in Type 3 the effective ramp was built only by silicone thickening and not by addition of sand slices (Fig. 6d).

In a similar fashion, vertical amplitude (dh) of the thrust anticline and horizontal displacement (ds) along the upper flat showed a clear dependence on the frontal ramp angle α. The ratio dh/ds progressively increased with increasing α-values in all types of models, indicating that a higher frontal ramp angle would favour a higher vertical growth of the thrust anticline, while low α-values favour a higher horizontal displacement along the upper flat (Fig. 7a, c). dh/ds ratios are markedly higher in Type 1 than in Type 2 and 3 models, although for $\alpha = 30^\circ$, the highest dh/ds value occurred in Type 3, showing a sharp deviation from the general trend (Fig. 7c). This is presumably because Type 3 configuration favoured collapse, upon reaching its angle of repose, of the growing anticline, while the hanging wall is overthrusting its own debris.

This leads to an increase of the ramp length because the hanging wall uses the protruding ductile layer to step-up its own debris, causing a comparative increase of dh. In any case, the higher dh/ds values exhibited by Type 1 with respect to Type 2 and 3 models appear to be strongly controlled by basal friction. This mechanism was previously identified in shortened sand wedges where for the same amount of shortening the ratio wedge length to wedge height increased with decreasing basal friction (Mulugeta, 1988; Colletta et al., 1991).

Accommodation styles above rigid ramps described in this paper are very similar to Merle and Abidi (1995) experiments, although in those models deformation was by pushing the sand (or sand–silicone) pack over a rigid ramp restricted to a frontal dip of 30°. In their experimental set-up with silicone above the lower flat and with a brittle/ductile thickness ratio of 5 (which can be approximated by our Type 2, $\alpha = 30°$, model), back thrusts developed above the rigid ramp. However, synshortening erosion of the hanging wall inhibited the development of back thrusts (see their Fig. 4). By comparison, in our Type 2 and $\alpha = 30°$ experiment, back thrusting did not take place even without erosion (Figs. 5b and 7). This difference in structural style, such as the development of back thrusts, for the same initial model configuration, might be related to the different way of end loading. In Merle and Abidi's experiments the rigid ramp was stationary and the sand pack was pushed from the rear to overthrust it, while in our experiments the opposite was true—i.e. the rigid ramp underthrusts the sand pack.

4.1. Limitation of the models

The present models consider only hanging wall accommodation styles above rigid staircase footwalls. Although such a model design allows exploration of a wide spectrum of ramp dips it has the disadvantage that it does not consider development of smooth-trajectory thrusts, which also occur in nature (Cooper and Trayner, 1986). Moreover, the models have assumed a high strength contrast between the deforming sediments in the hanging wall and the rigid ramp, representing either a thrust footwall or a pre-existing basement fault. An additional limitation of our models is that the rigid footwall does not deform and consequently does not undergo any rotation during the progressive deformation, as happens in natural thrust systems and in thrust sand wedge models (e.g. Mulugeta, 1988; Mulugeta and Koyi, 1987, 1992). This is perhaps our greatest simplification of natural situations, where the footwall may also take part in the deformation during thrust sheet evolution. However, our models were exclusively intended to address hanging wall accommodation styles above thrust ramps with variable inclination angle and not the propa-

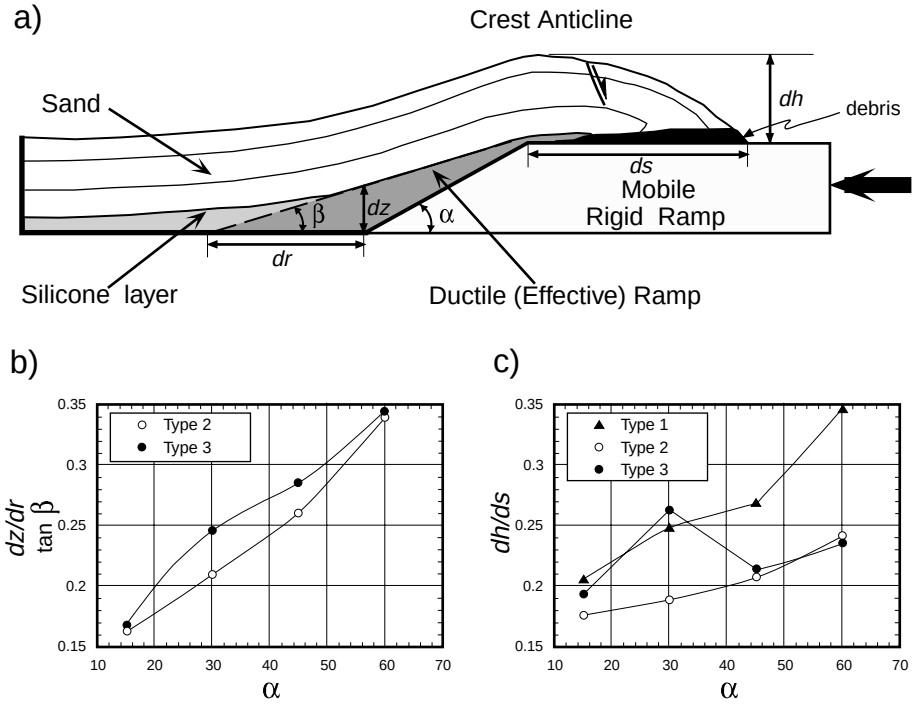

Fig. 7. Geometrical characteristics of ductile ramps (b) and model thrust anticlines (c) in relation to the frontal rigid ramp angle α. Parameters used in the diagrams are shown in (a) (line drawing of Type 2 model, $\alpha = 30°$).

gation (or rotation) of thrust ramps. In any case, despite the above limitations, the analogue modelling results discussed in the present paper provide some valuable insights into the mechanics of hanging wall accommodation above thrust ramps, and can also be compared with some natural examples.

4.2. Comparison with geological examples

The influence of the rigid footwall ramp on the hanging walls geometry needs to be evaluated for a correct comparison of the experimental results to nature. Generally, the marked lateral strength variation introduced by the rigid ramp makes our models suitable for studying thrust ramps developed above pre-existing normal faults juxtaposing rigid rocks (e.g. the basement or a rigid cover beam) with weak rocks (e.g. evaporites or shales) composing a décollement layer. In this case, the thrust detachment along the décollement is blocked by propagating into the rigid basement (or rigid cover beam), such that the sediments of the hanging wall undergo strong deformation (e.g. 'buttressing' phenomena; Gillcrist et al., 1987; Schedl and Wiltschko, 1987; Welbon, 1988; Butler, 1989). Thrust ramps with angles higher than 30° can also be generated by rotation during progressive shortening (see discussion in Mulugeta and Koyi, 1992), but the study of such a process is not allowed by our experimental design.

Generally, the dip of pre-existing normal faults is higher than 45° (mostly it is around 60°), such that some of the inferences in structural pattern of thrust ramps suggested by modelling of $\alpha \geq 45°$ can be directly applied to these geological situations. Indeed, deformation patterns of model hanging walls with $\alpha \geq 45°$ compare well with those of natural fault-controlled

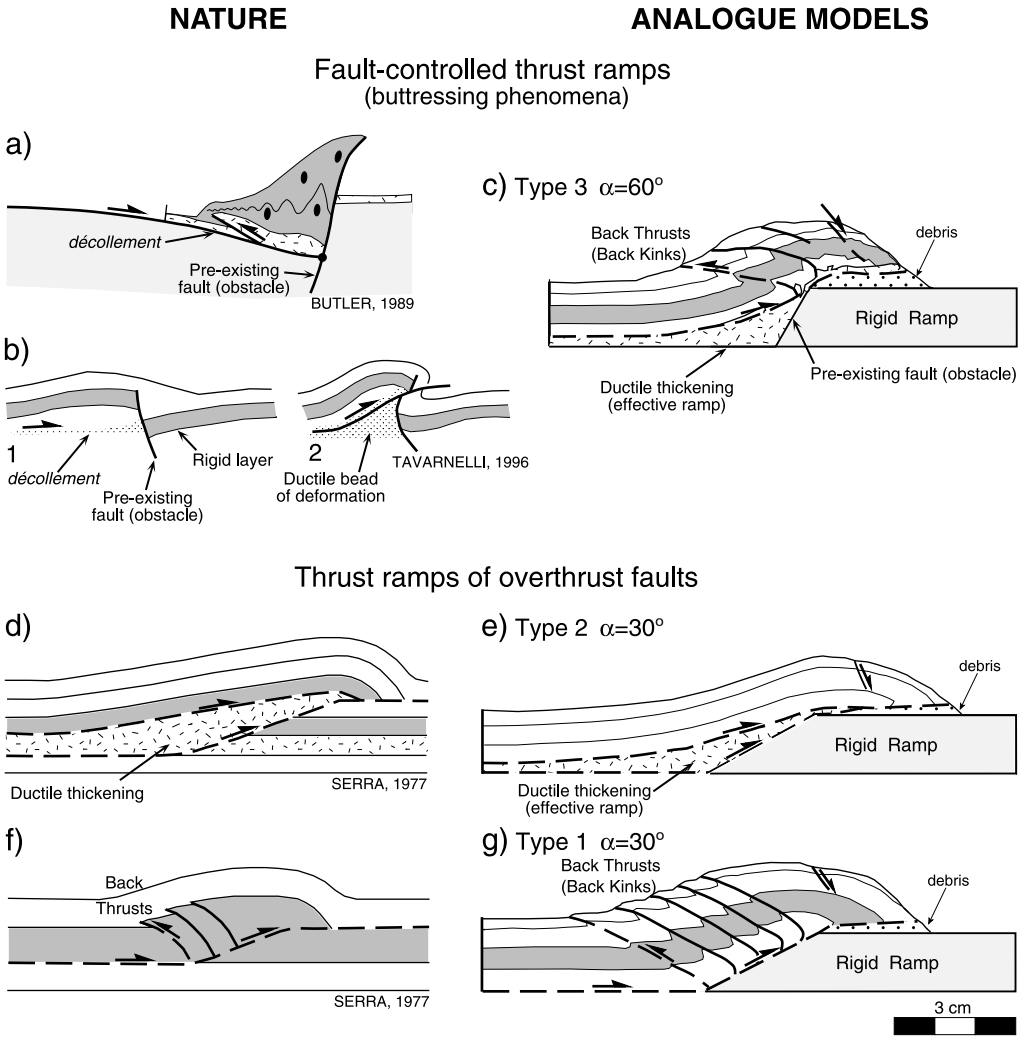

Fig. 8. Comparison between natural thrust ramps (a, b, d, f) and models shown in this work (c, e, g); dashed lines indicate movement along active faults. Figure (a) is redrawn after Butler (1989), (b) after Tavarnelli (1996), (d) and (f) after Serra (1977).

thrust ramps which exhibit typical characteristics, such as back thrusts, intense folding and strain intensification indicating substantial vertical pure shear stretching (cf. Fig. 8a–b with c).

Regarding the comparison of the models with ramp regions of overthrust faults, by choosing this model set-up we have assumed that the thrust fault, represented by the face of the rigid ramp, has propagated rapidly at the onset of deformation, and only after the development of the ramp has the hanging wall started to thrust over an undeformable footwall. These assumptions are also at the base of analytical models, which have been successfully applied to natural cases, quantifying the geometry and deformation of ductile layer-based hanging walls in thrust ramp regions (Taboada et al., 1990; Jordan and Noack, 1992). Indeed, the mechanical behaviour of our models is very similar to that formulated in the analytical models, such as the development of a wedge-like inclusion of ductile material above the ramp which closely matches our ductile (effective) ramp in Type 2 and 3 models (cf. model Type 2 with $\alpha = 30^\circ$ in Figs. 5b and 7a with fig. 2b–c in Jordan and Noack, 1992, where a 30°-dipping ramp is also assumed).

Considering that thrust ramps mostly develop at an inclination of about 30° to the maximum principal stress axis σ_1 (sub-horizontal in compressive regime) and that in our models $\theta \preceq 30^\circ$ (see Section 3.1), we are confident that the effect of having a rigid ramp with $\alpha \leq 30^\circ$ (instead of a sand–silicone footwall ramp) on the hanging wall geometry would be negligible, while the applicability of models with $\alpha \geq 45^\circ$ should be restricted to thrust ramps controlled by pre-existing normal faults. This hypothesis is also supported by the analogue models (both with and without silicone at the base) incorporating a 30°-dipping rigid ramp reported in Merle and Abidi (1995); indeed, in these models the hanging wall above the rigid ramp shows a deformation style which is comparable to that observed above an ~30°-dipping footwall ramp composed of the same material as the hanging wall. When the hanging wall is underlain by a ductile layer, the effect of having a rigid ramp (for $\alpha \leq 30^\circ$) would be even smaller because, as noted by Jordan and Noack (1992), the change in thickness of the ductile layer in the vicinity of the ramp has an important influence on hanging wall geometry, which is not therefore simply (directly) related to the geometry of the footwall ramp. In addition, the presence of a weak basal layer implies that the inclination of the σ_1 axis is very close to horizontal (e.g. Davis and Engelder, 1985), such that the hinterland-dipping fault plane practically coincides with the 30°-dipping rigid ramp.

Analysis of model results and structural features of overthrust faults suggest that both in nature and in experiments deformational style above thrust ramps appears to be strongly influenced by the overall hanging wall rheology. For instance, we have shown that the occurrence of incompetent material at the base of the models inhibits the formation of back thrusts in the hanging wall. This structural evolution has also been documented in nature, as no significant back thrust development takes place when ductile rocks occur at the base of hanging walls in well-exposed outcrop-scale thrust ramps (e.g. Serra, 1977; Fig. 8d).

In addition, the development of a ductile (effective) ramp in Type 2 and 3 models strikingly matches the ductile thickening by cataclastic flow of incompetent rocks (evaporites and shales) at the base of thrust sheets in natural thrust ramp regions (e.g. Serra, 1977; Cooper and Trayner, 1986; Fig. 8d–e), as well as in fault-controlled thrust ramps (e.g. Tavarnelli, 1996). In these cases, the ductile ramp (or back-limb) is typically longer and flatter than the rigid ramp. Note also that in both models and nature, the movement appears to occur along the lower flat as well as along the upper contact of the ductile layer, so that the more competent rocks glide over the thickened ductile ramp (Fig. 8d–e).

Regarding the purely frictional hanging walls, the development of a series of back thrusts in natural thrust ramps (e.g. Serra, 1977; Mandl and Crans, 1981) is directly comparable to Type 1 models (Fig. 8f–g). In addition, the warped trajectory of the back thrusts in the model is similar to that in nature. This geometry is presumably strongly controlled by the high friction along the ramp, as well as by the homogeneity of the hanging wall. Type 1 models might also simulate the conditions of a thrust reactivated at upper structural levels, where fluid pressure is declining and friction along the thrust plane is dramatically increasing. Indeed, back thrusting is typical of high structural levels and dominates the late stage of emplacement of thrust sheets (e.g. Cello and Nur, 1988).

The present models also have implications for the geometrical characteristics of natural thrust surfaces as well as for the modes of deformation in ramp regions of overthrust faults. Cooper and Trayner (1986) concluded that smooth-trajectory thrusts can often occur in nature, and together with the staircase geometry represent two end members in a continuous range of possible thrust profiles. In frictional hanging walls (Type 1) the system was forced to follow the staircase trajectory, and accommodation of bulk compression progressed by development of a series of stacked back thrusts at different α. In models with silicone at the base, the system configured a ductile ramp, which is markedly similar to that of smooth-trajectory thrusts as proposed by Cooper and Trayner (1986). Based on these observations, our models might indicate that the presence of ductile members at the bottom of a thrust sheet would favour movement along a smooth-trajec-

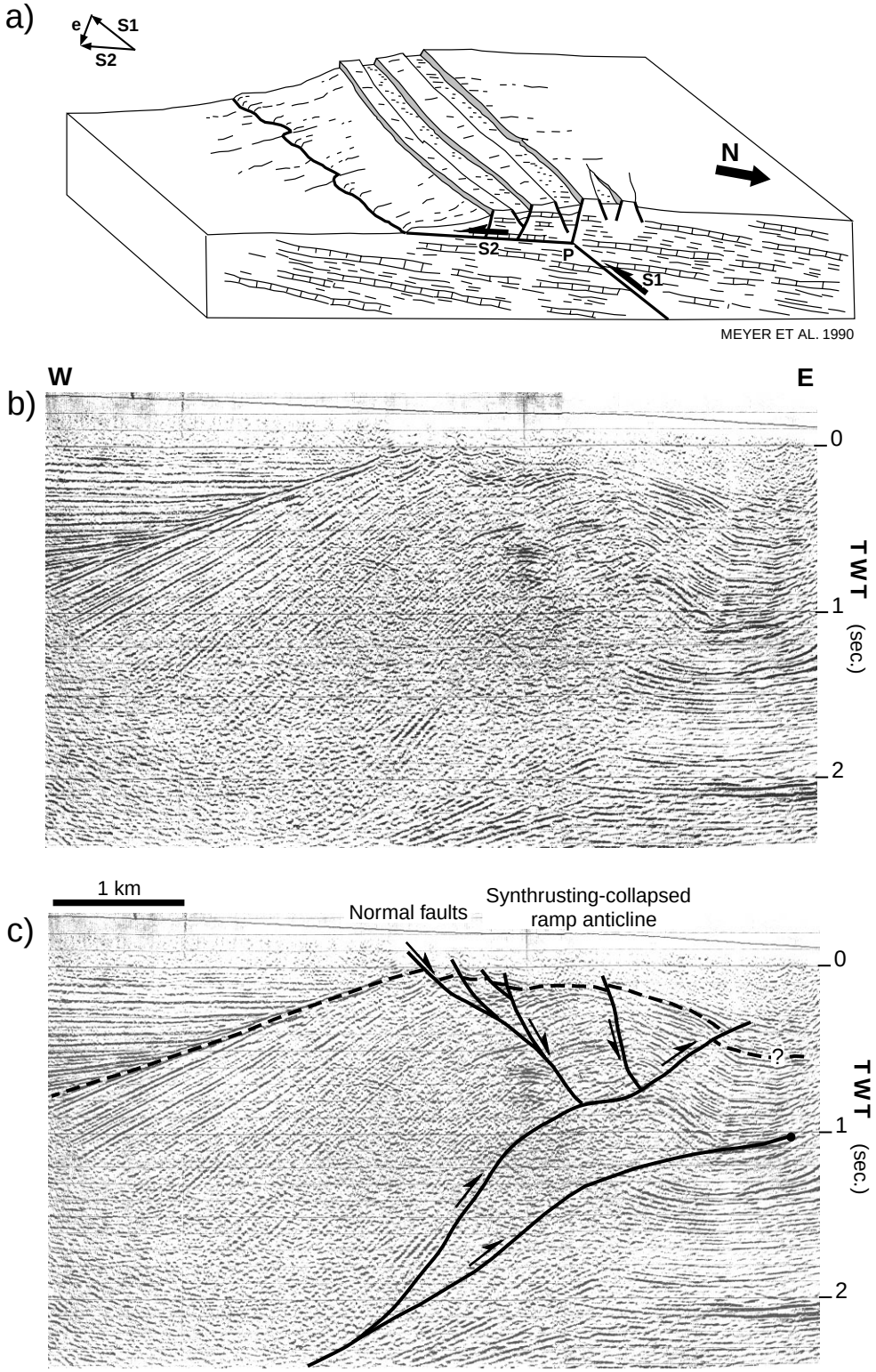

Fig. 9. Examples of normal faulting associated with synchronous thrusting at shallow structural levels. (a) Deformations induced by the El Asnam earthquake (redrawn from Meyer et al., 1990); S1 and S2 are the slip vectors of the two thrust segments, while *e* is the component of extension accommodated by the normal faults. (b, c) Normal faults affecting the crest of a growing thrust anticline in the Pliocene Adriatic Foredeep of the Umbria–Marche Apennines (Italy) (seismic line by courtesy of FINA Italiana S.p.A.); (b) uninterpreted and (c) interpreted version of the seismic profile.

tory thrust but not back thrusting. Finally, Cooper and Trayner (1986) also hypothesised that deformation at the ramp region of thrust faults would have been mainly accommodated by ductile deformation in the footwall ramp. This mechanism appears to be very similar to the ductile thickening described in Type 2 and 3 models, as well as to the thickening observed in the lowest sand layers (in front of the rigid ramp) in Type 1 models.

4.3. Syn-thrusting gravitational collapse of ramp anticlines

Foreland-dipping normal faults commonly develop at the crest of anticlines in all types of models. These normal faults develop synchronously with the thrusting as second-order structures along the ramp and upper flat. Typically, the geometry of normal faulting depends on the initial model configuration such as the ramp inclination angle α and the type of model (see Figs. 2, 5 and 6).

A similar process has also been identified in some geological examples, like the deformations associated with the El Asnam (Algeria) earthquake (M = 7.3) of the 10th October 1980. During that event, SE-directed thrusting was accompanied by the development of major SE-dipping normal faults, which were commonly associated with antithetic faults (King and Vita-Finzi, 1981; Philip and Meghraoui, 1983; Meyer et al., 1990; Fig. 9a). The geometry of normal faulting appears to be controlled by the bending of the thrust surface (at point P), which becomes gentler upwards (Meyer et al., 1990; Fig. 9a). Indeed, the normal faults predominantly affected the thrust sheet located above the upper gently dipping thrust segment (S2; Fig. 9a). This mechanism can be compared with our models, where point P corresponds to the intersection line between the rigid ramp and the upper flat, with the normal faults affecting the thrust sheet above the upper flat (see Figs. 2a–c, 3, 5b–d and 6d).

Furthermore, the occurrence of normal faulting synchronously with thrusting is revealed by the analysis of a seismic line in the Adriatic foredeep (Northern Apennines, Italy; Fig. 9b–c). The normal faults affect the crest of the ramp anticline related to a high-angle W-dipping thrust-fault, whose syn-sedimentary activity is demonstrated by the architecture of the syn-tectonic strata which show clear onlap relationships to the backlimb of the growing anticline (Fig. 9b–c). Notice also that the normal faults appear again to be controlled by the profile of thrust surface, as normal faults form where the thrust surface flatten upsection.

This process of extension associated with active thrust sheets involves the collapse of the upper portion of the hanging wall and it is likely to occur mostly at upper structural levels. In this frame, we have shown in Section 3.1 that normal faulting along pre-existing back thrust faults is a possible mechanism for internal deformation of thrust sheets, which should be taken into account when studying natural thrust systems.

In this process gravity plays a major role in favouring the creation (or the reactivation of earlier structures) of normal faults to accommodate the extension during movement of the thrust sheet above the upper flat (or the gently dipping thrust surface in the natural examples). This process is likely to take place when the thrust sheet is laterally unconfined toward the foreland

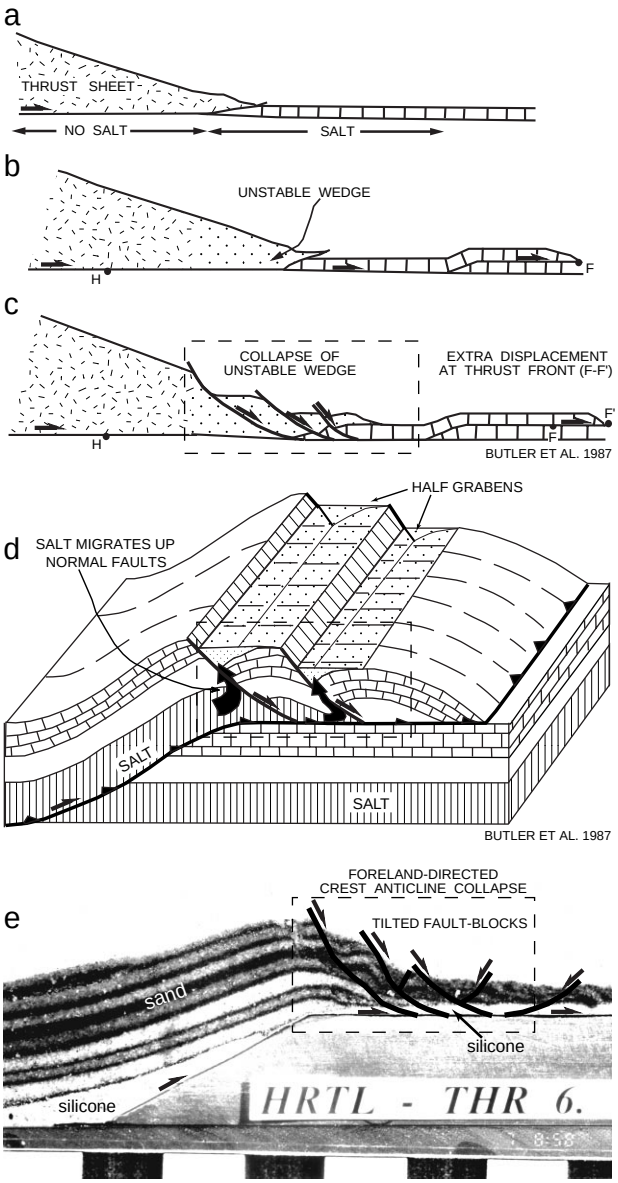

Fig. 10. Gravitational collapse of unstable thrust wedge above Cambrian salt at the Himalayan Mountain Front (a–d are redrawn from Butler et al., 1987). A very similar pattern of tilted fault-blocks also results in the analogue model (e) when the growing anticline slides along the silicone above the upper flat; (e) is a close-up of the model shown in Fig. 6(e).

and the system is allowed to spread over the footwall. Similarly, the growing anticline shown in the seismic profile of the Apennine foredeep might have been weakly constrained laterally toward the foreland by semi-consolidated sediments (Fig. 9b–c).

A particular case of normal faulting associated with thrusting is illustrated by the spectacular normal faults occurring at the Himalaya Mountain Front, where the thrust wedge glides over Cambrian salt (Butler et al., 1987; Fig. 10a–d). The resulting structural pattern consists of tilted fault-blocks affecting the front of the advancing thrust wedge, that becomes unstable and gravitationally collapses above the ductile salt (Fig. 10a–d). The structural style of the model illustrated in Fig. 10(e) is very similar to this example. Though the initial boundary conditions of the model differ slightly from the natural prototype (see Section 3.3), the kinematics of both processes is essentially equivalent (Fig. 10), thus supporting the hypothesis that the normal faults at the Himalaya front formed contemporaneously with the thrusting.

5. Conclusions

Results of scaled sand and sand–silicone models shortened over a rigid ramp–flat footwall suggest the following main conclusions:

1. Style of hanging wall accommodation depends upon the overall thrust sheet rheology as well as upon the ramp inclination angle α. Rheology of hanging wall is far more important than the ramp angle α in controlling the deformation above rigid ramps; while the presence of a ductile layer at the base of the sand prevents the formation of back thrusts for gentle to moderate dips ($\alpha = 15$–30° in Type 2 and $\alpha = 15$–45° in Type 3 models), these developed in frictional hanging walls irrespective of the ramp angle.
2. Type 2 and 3 models spontaneously configured a ductile (effective) ramp in front of the rigid ramp. The inclination angle β of the ductile ramp increased with α and provided an easy glide horizon for the brittle hanging wall to climb over the rigid ramp.
3. The analogue models exhibit some marked similarities with geological examples of hanging walls gliding over a frontal ramp. These concern natural thrust ramps of overthrust faults with $\alpha \leq 30^\circ$, as well as thrust ramps whose location was controlled by pre-existing normal faults with inclination $\alpha \geq 45^\circ$.
4. The models emphasise the importance of the ductile thickening in front of rigid footwall ramps (i.e. development of ductile ramps) in controlling the deformation geometry of the sediments in the hanging wall.
5. Foreland-directed normal faulting can develop on the crest of growing thrust-related ramp anticlines, as illustrated in models compared with some geological examples.
6. Finally, the model results suggest that extensional reactivation of early back thrusts may take place during the emplacement of a thrust sheet and may represent an important deformational mechanism.

Acknowledgements

We thank Prof. G. Mitra and Dr. D.A. Medwedeff for the constructive review of the manuscript and Prof. C.J. Talbot and Dr. F. Sani for helpful discussions. MB wishes to thank FINA Italiana S.p.A. (especially Drs. J. Staffurth, P. Dattilo and C. Turrini) for the permission to publish the seismic profile illustrated in Fig. 9. Research funded by CNR "Centro di Studio di Geologia dell'Appennino e delle Catene Perimediterranee" (Publ. No. 332) and MURST 40% grants (responsible Prof. P. Manetti).

References

Allen, P.A., Crampton, S.L., Sinclair, H.D., 1991. The inception and early evolution of the North Alpine foreland basin, Switzerland. Basin Research 3, 143–163.

Anderson, E.M., 1951. The Dynamics of Faulting and Dyke Formation. Olivier and Boyd, Edinburgh.

Berger, P., Johnson, A.M., 1980. Fist-order analysis of deformation of a thrust sheet moving over a ramp. Tectonophysics 70, T9–T24.

Beutner, E.C., Fisher, D.M., Kirkpatrik, J.L., 1988. Kinematics of deformation at a thrust fault ramp from syntectonic fibers in pressure shadows. Geological Society of America Special Paper 222, 77–88.

Bombolakis, E.G., 1986. Thrust-fault mechanics and origin of a frontal ramp. Journal of Structural Geology 8, 281–290.

Boyer, S.E., Elliot, D., 1982. Thrust systems. American Association of Petroleum Geologists Bulletin 66, 1196–1230.

Butler, R.W.H., 1982. The terminology of structures in thrust belts. Journal of Structural Geology 4, 239–245.

Butler, R.W.H., 1989. The influence of pre-existing basin structure on thrust system evolution in the Western Alps. In: Cooper, M.A., Williams, G.D. (Eds.), Inversion Tectonics, Geological Society of London Special Publication, 44, pp. 105–122.

Butler, R.W.H., Coward, M.P., Harwood, G.M., Knipe, R.J., 1987. Salt control on thrust geometry, structural style and gravitational collapse along the Himalayan Mountain Front in the Salt Range of Northern Pakistan. In: Lerche, I., O'Brien, J.J. (Eds.), Dynamical Geology of Salt and Related Structures. Academic Press, pp. 339–418.

Byerlee, J.D., 1978. Friction of rocks. Pure Applied Geophysics 116, 615–626.

Carter, N.L., Hansen, F.D., 1983. Creep of rocksalt. Tectonophysics 92, 275–333.

Cello, G., Nur, A., 1988. Emplacement of foreland thrust systems. Tectonics 7, 261–271.

Colletta, B., Letouzey, J., Pinedo, R., Ballard, J.F., Balé, P., 1991. Computerized X-ray tomography analysis of sandbox models: Examples of thin-skinned thrust systems. Geology 19, 1063–1067.

Cooper, A., Trayner, P., 1986. Thrust-related geometry: implications for thrust-belt evolution and section-balancing techniques. Journal of Structural Geology 8, 305–312.

Davis, D.M., Engelder, T., 1985. The role of salt in fold-and-thrust belts. Tectonophysics 119, 67–88.

Dahlstrom, C.D.A., 1970. Structural geology in the eastern margin of the Canadian Rocky Mountains. Canadian Petroleum Geology Bulletin 18, 332–406.

Eisenstadt, G., De Paor, D.G., 1987. Alternative model of thrust-fault propagation. Geology 15, 630–633.

Elliott, D., 1976. The energy balance and deformation mechanisms of thrust sheets. Philosophical Transactions Royal Society of London A282, 289–312.

Faccenna, C., Nalpas, T., Brun, J.P., Davy, P., Bosi, V., 1995. The influence of pre-existing thrust faults on normal fault geometry in nature and in experiments. Journal of Structural Geology 17, 1139–1149.

Gillcrist, R., Coward, M., Mugnier, J.L., 1987. Structural inversion and its controls: examples from the Alpine foreland and the French Alps. Geodinamica Acta 1, 5–34.

Gretener, P.E., 1972. Thoughts on overthrust faulting in a layered sequence. Canadian Petroleum Geology Bulletin 20, 583–607.

Gretener, P.E., 1981. Pore pressure, discontinuities, isostasy and overthrust. In: McClay, K., Price, N.J. (Eds.), Thrust and Nappe Tectonics, Geological Society of London Special Publication, 9, pp. 33–39.

Harris, L.D., Milici, R.D., 1977. Characteristics of thin-skinned style deformation in the southern Appalachians, and potential hydrocarbon traps. U.S. Geological Survey Professional Paper 1018.

Hoshino, K., Koide, H., Inami, K., Iwamura, S., Mitsui, S., 1972. Mechanical properties of Japanese Tertiary sedimentary rocks under high confining pressure. Geological Survey of Japan Report 244.

Hubbert, M.K., 1937. Theory of scale models as applied to the study of geologic structures. Geological Society of America Bulletin 48, 1459–1520.

Jaeger, J.C., Cook, N.G.W., 1979. Fundamentals of Rock Mechanics. Chapman and Hall, London.

Jordan, P., Noack, T., 1992. Hangingwall geometry of overthrust emanating from ductile decollements. In: McClay, K.R. (Ed.), Thrust Tectonics. Chapman and Hall, pp. 311–318.

King, G.C.P., Vita-Finzi, C., 1981. Active folding in the Algerian earthquake of 10 October 1980. Nature 292, 22–26.

Krantz, R.W., 1991a. Normal fault geometry and fault reactivation in tectonic inversion experiments. In: Roberts, A.M., Yielding, G., Freeman, B. (Eds.), The Geometry of Normal Faults, Geological Society of London Special Publication, 56, pp. 219–229.

Krantz, R.W., 1991b. Measurements of friction coefficients and cohesion for faulting and fault reactivation in laboratory models using sand and sand mixtures. In: Cobbold, P.R. (Ed.), Experimental and Numerical Modelling of Continental Deformation, Tectonophysics, 188, pp. 203–207.

Kukal, Z., 1990. The rate of geological processes. Earth-Science Review 28, 8–284.

Mandl, C., Crans, W., 1981. Gravitational gliding in deltas. In: McClay, K., Price, N.J. (Eds.), Thrust and Nappe Tectonics, Geological Society of London Special Publication, 9, pp. 41–54.

Merle, O., Abidi, N., 1995. Approche expérimentale du functionnement des rampes émergentes. Bulletin de la Société Géologique de France 166, 439–450.

Meyer, B., Avouac, P., Tapponnier, P., Meghraoui, M., 1990. Mesures topographiques sur le segment SW de la zone faillée d'El Asnam et interprétation mécanique des relations entre failles inverses et normales. Bulletin de la Société Géologique de France 8, 447–456.

Mitra, S., 1986. Duplex structures and imbricate thrust systems: geometry, structural position, and hydrocarbon potential. American Association of Petroleum Geologists Bulletin 70, 1087–1112.

Mulugeta, G., 1988. Modelling the geometry of Coulomb thrust wedges. Journal of Structural Geology 10, 847–859.

Mulugeta, G., Koyi, H., 1987. Three-dimensional geometry and kinematics of experimental piggyback thrusting. Geology 15, 1052–1056.

Mulugeta, G., Koyi, H., 1992. Episodic accretion and strain partitioning in a model sand wedge. Tectonophysics 202, 319–333.

Philip, H., Meghraoui, M., 1983. Structural analysis and interpretation of the surface deformation of El Asnam earthquake of October 10, 1980. Tectonics 2, 17–49.

Ranalli, G., Yin, Z.-M., 1990. Critical stress difference and orientation of faults rocks with strength anisotropies: the two-dimensional case. Journal of Structural Geology 12, 1067–1071.

Rich, J.L., 1934. Mechanics of low-angle overthrust faulting illustrated by Cumberland thrust block, Virginia, Kentucky and Tennessee. American Association of Petroleum Geologists Bulletin 18, 1584–1596.

Schedl, A., Wiltschko, D.V., 1987. Possible effects of pre-existing basement topography on thrust fault ramping. Journal of Structural Geology 9, 1029–1037.

Serra, S., 1977. Styles of deformation in the ramp regions of overthrust faults. In: Twenty-Ninth Annual Field Conference—1977—Wyoming Geological Association Guidebook, pp. 487–498.

Sibson, R.H., 1974. Frictional constraints on thrust, wrench and normal faults. Nature 249, 542–544.

Sibson, R.H., 1985. A note on fault reactivation. Journal of Structural Geology 7, 751–754.

Suppe, J., 1983. Geometry and kinematics of fault-bend folding. American Journal of Science 283, 684–721.

Taboada, A., Ritz, J.F., Malavieille, J., 1990. Effect of ramp geometry on deformation in a ductile decollement level. Journal of Structural Geology 12, 297–302.

Tavarnelli, E., 1996. Ancient synsedimentary structural control on thrust ramp development: an example from the Northern Apennines, Italy. Terra Nova 8, 65–74.

Weijermars, R., 1997. Principles of Rock Mechanics. Alboran Science Publishing, Amsterdam.

Weijermars, R., Jackson, M.P.A., Vendeville, B., 1993. Rheological and tectonic modeling of salt provinces. Tectonophysics 217, 143–174.

Welbon, A., 1988. The influence of intra-basinal faults on the development of a linked thrust system. Geologische Rundschau 77, 11–24.

Wiltschko, D.V., 1979. Mechanical model for thrust sheet deformation at a ramp. Journal of Geophysical Research 84, 1091–1104.

Wiltschko, D.V., 1981. Thrust sheet deformation at a ramp: summary and extension of an earlier model. In: McClay, K., Price, N.J. (Eds.), Thrust and Nappe Tectonics, Geological Society of London Special Publication, 9, pp. 55–63.

Zapata, T.R., Allmendinger, R.W., 1996. Growth stratal records of instantaneous and progressive limb rotation in the Precordilleran thrust belt and Bermejo basin, Argentina. Tectonics 15, 1065–1083.